Indian Journal of Pure & Applied Physics
Vol. 64, October 2026, pp. 1107-1116
DOI: 10.56042/ijpap.v64i10.30528

Estimation of Global Solar Radiation in the Eastern Terai Region of Nepal using Meteorological Parameters in RadEst 3.0

Basanta Kumar Rajbanshi[a*], Ram Gopal Singh[a], Anima Kumari Singh Rajbanshi[b] & Bed Raj K C[c]

[a]Faculty of Physical Sciences, Shri Ramswaroop Memorial University, Barabanki 225 001, India

[b]Department of Chemistry, Tri-Chandra Campus, Tribhuvan University, Kathmandu 446 05, Nepal

[c]Pokhara University, Kaski, Gandaki Province 337 00, Nepal

Received: 8th April 2026; accepted: 27th August 2026

Understanding the distribution of solar radiation is essential for the development and optimisation of solar energy technologies. This study estimates daily global solar radiation (GSR) in Janakpur, a city in the Eastern Terai Region of Nepal, using RadEst 3.0 software. The analysis used seven meteorological parameters: rainfall, maximum and minimum temperatures, maximum and minimum humidity, and wind speed, with global solar radiation measurement for model validation.

Four empirical models were employed: Donatelli and Bellocchi (DB), Campbell and Donatelli (CD), Bristow and Campbell (BC), and the combined Donatelli-Campbell-Bristow-Bellocchi (DCBB). Their performance was evaluated using statistical metrics including the coefficient of determination (R^2), mean bias error (MBE), mean percentage error (MPE), mean error (ME), root mean square error (RMSE), and correlation coefficient (r). Parameter fitting (PF) was applied to optimize model performance by maximizing R^2 and minimizing CRM and RMSE. The annual mean GSR was 12.9 ± 0.25, 16.3 ± 0.27, 14.7 ± 0.33, and 15.3 ± 0.33 MJ/m²/day for 2021, 2022, 2023, and 2024, respectively, with maximum daily values of 26.4, 28.3, 27.7, and 26.4 MJ/m²/day.

Among the models, DCBB consistently outperformed others, yielding R^2 values of 0.37, 0.63, 0.62, and 0.69, and RMSE values of 2.54, 2.13, 2.77, and 2.64 MJ/m²/day for the respective years. Additionally, DCBB showed the lowest MBE and MPE values across all years. Therefore, the DCBB model is identified as the most reliable for accurate GSR estimation in this region of Nepal.

Keywords*:* RadEst 3.0 software, Air transmissivity, Atmospheric variables, Pyranometer, Global solar radiation

1 Introduction

Nepal, a landlocked country bordered by China and India, exhibits highly diverse topography, ranging from the high Himalayas to mid-hills and the Terai plains. Covering an area of 147,516 km², with dimensions of approximately 800 km in length and 200 km in width, Nepal lies between latitudes 26°22′-30°27′ N and longitudes 80°4′-88°12′ E. The country's elevation changes dramatically over short distances, strongly influencing geomorphology, climate, and biodiversity. Its location in a solar energy favorable belt, combined with over 300 sunny days per year and an average daily sunshine duration of 6.8 hours[1], indicates significant potential for solar energy development. However, Nepal's limited fossil fuel resources have contributed to persistent energy deficits and economic challenges.

According to the Energy Sector Synopsis Report 2024, Nepal has an estimated potential of approximately 2,100 MW for grid-connected solar PV, consistent with earlier SWERA assessments[2]. Despite this, only 106.7 MW has been grid-connected, while more than 1.1 million off-grid solar home systems contribute roughly 30 MWp in rural areas[3]. During the fiscal year 2022/23, total energy consumption reached 532.4 PJ, dominated by traditional biomass (63.9 %), with modern renewables contributing only 3.1 %, and commercial energy (grid electricity and fossil fuels) accounting for 33 %[4]. Although electricity access has expanded to 97.7 % of the population, about 5.9 % still rely on off-grid renewable energy, highlighting the critical need to optimize local renewable energy resources, particularly solar energy[5].

GSR is a key determinant of solar energy potential and can be estimated through empirical, hybrid, and machine-learning approaches. Classical models, such as the Angstrom-Prescott sunshine-based model[6,7], remain widely used due to their simplicity and reliability. Other approaches include temperature-based models[8, 9], hybrid models combining sunshine

*Corresponding author: E-mail: basantaraz05@gmail.com

and temperature data[10, 11], and recent AI-driven techniques integrating geographic and meteorological parameters[12].

Regional studies have highlighted substantial spatial and temporal variability in GSR. For example, Oulimar et al. reported strong seasonal fluctuations in southern Algeria, with daily radiation exceeding 6.16 kWh/m² [13], while Pinto demonstrated high accuracy of PV-panel-based estimations compared to NASA POWER and Sun DATA systems[14]. In Nepal, empirical studies have mostly focused on selected urban and highland areas, often using RadEst 3.0 software for daily and monthly GSR estimation. Early work covered Simara and Kathmandu, followed by studies in Jumla[15], Khumaltar, Simikot[16], Dhankuta, Biratnagar, Taplejung, and Okhaldhunga and Jiri. Some studies, explored hybrid empirical machine learning methods to improve prediction accuracy.

Recent studies have further highlighted the effectiveness of artificial intelligence (AI) and machine learning (ML) techniques for estimating and forecasting solar radiation by integrating geographic and meteorological parameters. For instance, multiple ML and deep learning models using long-term datasets and found Gradient Boosting and RNN to be most effective[17]. Similarly, temperature, wind speed, and surface pressure strongly influence solar irradiance prediction in Rajasthan, with Random Forest models achieving high accuracy[18]. Hybrid approaches, such as combining sky-camera images with meteorological data through neural networks, have also improved short-term forecasting accuracy. Collectively, these findings indicate that ML-based models, particularly ensemble and temporal learning methods, can significantly enhance the reliability of solar radiation prediction.

This study analyzes the temporal distribution of solar energy in Janakpur using local meteorological datasets and four RadEst 3.0 empirical models: Bristow-Campbell (BC), Campbell-Donatelli (CD), Donatelli-Bellocchi (DB), and Donatelli-Campbell-Bristow-Bellocchi (DCBB). Using multi-year ground-based solar radiation and meteorological data from Janakpur, a humid, low-altitude Terai region of Nepal, the study systematically evaluates model performance, identifies the most accurate model, and examines interannual and seasonal variations in GSR in relation to key local climatic parameters. The findings provide valuable data for solar-resource assessment, energy planning, sustainable development, and future solar energy policies and investments in Nepal's Terai region.

2 Materials and Methods

2.1 Study Area

Janakpur (26.71° N, 85.92° E, 76 m above sea level), the capital of Madhesh Province, lies in Nepal's flat, southern Terai plains. It features a subtropical climate marked by hot summers, cool winters, and a strong monsoon-factors that directly govern local surface solar radiation. As a growing urban and agricultural hub, the area experiences significant atmospheric loading from construction dust, vehicular and industrial emissions, crop-residue burning, and transboundary aerosols, all of which scatter and absorb solar radiation, especially during dry and cloudy periods. The study site and meteorological station are shown in Fig. 1.

2.2 Data Sources

Meteorological data for Janakpur for the period 2021–2024 were obtained from the Department of Hydrology and Meteorology (DHM), Government of Nepal. The dataset included global solar radiation (GSR), maximum and minimum air temperatures, relative humidity, rainfall, and wind speed. GSR was measured using a CMP6 pyranometer, while temperature and rainfall were recorded using a maximum-minimum thermometer and a Udometer, respectively. The CMP6 pyranometer operates over a spectral range of 310-2800 nm and converts incident solar radiation into a measurable voltage signal.

These meteorological parameters were selected for their direct physical link to surface solar radiation. Temperature correlates positively with clear-sky radiation, whereas relative humidity and rainfall represent atmospheric moisture and cloud cover,



Fig. 1 — Location map of Janakpur, Dhanusha district, Nepal

typically exhibiting an inverse relationship with global solar radiation (GSR). Wind speed governs atmospheric mixing and cloud displacement, while daily temperature extremes (T_{max} and T_{min}) serve as proxies for ambient thermal dynamics. Together, these variables drive the performance of the empirical models evaluated in RadEst 3.0.

Hourly observations from Department of Hydrology and Meteorology (DHM) stations were converted to daily averages using Simpson's $1/3$ rule. Missing or anomalous values were minimal and were replaced using mean values from adjacent valid observations. This preprocessed, continuous daily dataset served as input for RadEst 3.0 model evaluation and comparison.

2.3 Modeling Tool

2.3.1 RadEst 3.0

RadEst 3.0 was employed to estimate daily GSR using meteorological inputs and geographic coordinates (latitude, longitude, altitude). The software incorporates four empirical models: Bristow & Campbell (BC), Campbell & Donatelli (CD)[19], Donatelli & Bellocchi (DB)[20], and Donatelli-Campbell-Bristow-Bellocchi (DCBB)[21] which relate daily solar radiation to temperature variations and other climatic factors.

These models estimate surface solar radiation from atmospheric transmissivity and potential solar radiation.

$$\text{Est Rad}_i = tt_i \text{ Pot Rad}_i$$

$$\text{Pot Red}_{doy} = 117.5 dd_2 \frac{h_s \text{Sin (lat) Sin (dec)} + \text{Cos (lat) Sin}(h_s)}{\pi} \quad \ldots (1)$$

This equation employs the following variables: the latitude of the observation point (lat) in degrees, solar declination (dec), the sun's distance (dd_2), and the duration of half a day (hs).

i Bristow and Campbell (BC) Model

The Bristow-Campbell model estimates daily solar radiation from the relationship between diurnal temperature range and atmospheric transmissivity. A larger temperature range generally indicates clearer skies and higher solar radiation, whereas a smaller range indicates cloudier conditions and lower radiation. Estimated atmospheric transmissivity is;

$$tt_i = \tau\left[1 - \exp\left(\frac{-b\,\Delta T_i^c}{\text{month}\ \Delta T}\right)\right] \quad \ldots (2)$$

Hence from the equation, the estimated radiation provided is given by;

$$\text{Est Red}_i = \tau\left[1 - \exp\left(\frac{-b\,\Delta T_i^c}{\text{month}\ \Delta T}\right)\right] \text{PotRed}_i \quad \ldots (3)$$

where,

$$\Delta T_i = T_{max_i} - \frac{T_{min_i} + T_{min\ (i+j)}}{2} \quad \ldots (4)$$

ii Campbell and Donatelli (CD) Model

The Campbell-Donatelli (CD) model refines the Bristow-Campbell model by adding a seasonal correction factor (Tnc) to improve transmissivity estimates. The model calculates transmissivity as;

$$tt_i = \tau\left[1 - \exp\left\{-b \times f\left(T_{avg}\right) \Delta T_i^2\ f(T_{min})\right\}\right] \quad \ldots (5)$$

Thus,

$$\text{Est Red}_i = \tau\left[1 - \exp\left\{-b \times f\left(T_{avg}\right) \Delta T_i^2\ f_1(T_{min})\ \text{PotRed}_i\right\}\right] \quad \ldots (6)$$

where,

$$T_{avg} = \frac{T_{max_i} + T_{min_i}}{2} \quad \ldots (7)$$

Donatelli and Bellocchi (DB) Model

The Donatelli-Bellocchi (DB) model estimates solar radiation from air temperature, using seasonal factors (c_1 and c_2) to account for changes in atmospheric clarity. The model determines transmissivity as;

$$tt_i = \tau\left[1 + f(i)\left[1 - \exp\left\{\frac{-b\,\Delta T^2}{\Delta T_{week}}\right\}\right]\right] \quad \ldots (8)$$

Providing radiation estimates as;

$$\text{EstRed}_i = \tau\left[1 + f(i)\left[1 - \exp\left\{\frac{-b\,\Delta T_i^2}{\Delta T_{week}}\right\}\right]\right] \text{PotRed}_i \quad \ldots (9)$$

where,

$$f(i) = c_1\left[\sin\left(i\,c_2\frac{\pi}{180}\right) + \cos\left\{i\,f(c_2)\frac{\pi}{180}\right\}\right] \quad \ldots (10)$$

$$f(c_2) = 1 - 1.90\,c_3 + 3.83 c_3^2 \quad \ldots (11)$$

$$c_3 = c_2 \text{ integer } (c_2) \quad \ldots (12)$$

iii Donatelli-Campbell-Bristow-Bellocchi (DCBB) Model

The fourth model, DCBB, accounts for seasonal changes in atmospheric conditions and can be simplified by adjusting its correction factors. The estimated transmissivity under these circumstances is;

$$tt_i = \tau\left[1 + f(i)\left[1 - \exp\left\{\frac{-b\,\Delta T^2 f(T_{min})}{\Delta T_{avg}}\right\}\right]\right] \quad \ldots (13)$$

which provides radiation estimates as;

$$\text{EstRed}_i = \tau\left[1 + f(i)\left[1 - \exp\left\{\frac{-b\,\Delta T_i^2 f(T_{min})}{\Delta T_{avg}}\right\}\right]\right]\text{PotRed}_i \quad \ldots (14)$$

where,

$$f(i) = c_1\left[\sin\left(i\,c_2\frac{\pi}{180}\right) + \cos\left\{i\,f(c_2)\frac{\pi}{180}\right\}\right]$$

$$f(c_2) = 1 - 1.90\,c_3 + 3.83c_3^2$$

$$f(T_{avg}) = 0.017\exp\left\{\exp\left(-0.053 \times T_{avg}\right)\right\} \quad \ldots (15)$$

where,

$$T_{avg} = \frac{T_{max_i} + T_{min_i}}{2}$$

$$f(T_{min}) = \exp\frac{T_{min}}{T_{nc}} \quad \ldots (16)$$

$$c_3 = c_2 \text{ integer } (c_2)$$

where,

tt_i = estimated atmospheric transmissivity

τ = clear sky transmissivity

ΔT = average monthly temperature

T_{max} = maximum daily air temperature

T_{min} = minimum daily air temperature

b = temperature range coefficient

c = highly sensitive empirical parameter

T_{nc} = thermal factor

c_1 = magnitude parameter for seasonal variation

c_2 = profile coefficient for seasonal variation

i = day number of the year, i = 1 to 365 or 366

$f(T_{avg})$ = average temperature function

$f(T_{min})$ = minimum temperature function

Est Rad_i = estimated radiation (MJ m^{-2} day^{-1})

$PotRad_i$ = Extraterrestrial radiation i.e. radiation beyond Earth's atmosphere (MJ $m^{-2}day^{-1}$)

2.4 Analysis Workflow, Calibration and Validation

The modeling workflow began by entering the latitude, longitude, and altitude of the Janakpur site into RadEst 3.0, followed by loading the prepared meteorological data in ASCII format. Clear-sky transmissivity was specified within the recommended range of 0.6–0.8. The selected RadEst 3.0 models were initially evaluated using the automatic optimization (AO) approach and subsequently calibrated using the parameter fitting (PF) approach. In PF calibration, the model parameters were adjusted using the observed GSR data so that the estimated radiation closely matched the measured values, particularly their average magnitude. This calibration helps reduce systematic bias and improve agreement between modeled and observed GSR.

The available daily meteorological and observed GSR data for Janakpur were divided into calibration and independent validation datasets. The calibration dataset was used to estimate the empirical coefficients of the RadEst 3.0 models, whereas the independent validation dataset was used to evaluate model performance. The calibration and validation datasets were kept separate to avoid evaluating model performance using the same observations used for coefficient estimation. Model performance was assessed using mean bias error (MBE), root mean square error (RMSE), mean percentage error (MPE), correlation coefficient (r), coefficient of residual mass (CRM), coefficient of determination (R^2), and coefficient of variation (CV). The best-performing model was identified based on its overall error statistics, consistency, correlation, and validation performance.

3 Results

3.1 Model Calibration and GSR Estimation

The auto-optimization tests revealed noticeable differences between measured and estimated GSR values, which prompted the calibration of four empirical models using Parameter Fitting (PF) with Janakpur's 2024 data. The objective was to maximise the coefficient of determination (R^2) while minimising errors (RMSE and CRM). Among the models, the DCBB model performed best, achieving an R^2 of 0.69, RMSE of 3.54 MJ/m²/day, and CRM of -0.08, indicating minimal bias and high reliability.

Using the calibrated parameters from 2024, the DCBB model was subsequently applied to estimate GSR for 2021-2023. The average annual GSR across the four years was 15.3 MJ/m²/day. Table 1 compares measured and estimated GSR values, showing that the DCBB model consistently outperformed the other models and closely matched observed data.

3.2 Statistical Error Analysis

A comparison of measured and estimated GSR (Table 2) confirmed the superior performance of the DCBB model across all years. Its R^2 values were 0.38 (2021), 0.63 (2022), 0.62 (2023), and 0.69 (2024). The model also produced lower RMSE, MBE, MPE, and CRM values, further demonstrating its accuracy and reliability.

3.3 Temporal Variation of GSR

Seasonal analysis showed that GSR peaked in spring, averaging 15.80 ± 0.47 MJ/m²/day (2021), 19.52 ± 0.30 (2022), 19.22 ± 0.55 (2023), and 19.63 ±

Table 1 — Measured and model-estimated average, maximum and total annual value of GSR at Janakpur

Year	Model	Average GSR (MJ/m^2 /day)			Maximum GSR (MJ/m^2 /day)			Total GSR (MJ/m^2)		
		AO	Mea	PF	AO	Mea	PF	AO	Mea	PF
	BC	16.0	15.3	15.3	26.9	26.4	26.7	5583	5583	5593
2024	CD	18.6	15.3	15.3	27.6	26.4	26.7	6788	5583	5594
	DB	15.9	15.3	15.3	31.8	26.4	31.2	5816	5583	5597
	DCBB	16.6	15.3	15.3	27.8	26.4	26.8	6051	5583	5580
	BC	15.2	14.7	15.3	26.5	27.7	26.6	5546	5373	5589
2023	CD	16.8	14.7	15.2	27.7	27.7	26.9	6144	5373	5563
	DB	14.8	14.7	15.3	27.7	27.7	29.1	5416	5373	5594
	DCBB	16.4	14.7	15.2	28.7	27.7	25.8	5996	5373	5548
	BC	16.7	16.3	14.9	26.4	28.3	25.1	6095	5956	5434
2022	CD	17.3	16.3	14.2	26.2	28.3	25.2	6331	5956	5185
	DB	16.2	16.3	14.8	23.6	28.3	28.0	5901	5956	5417
	DCBB	16.6	16.3	14.7	25.8	28.3	24.3	6065	5956	5353
	BC	12.9	12.9	14.7	24.8	26.4	26.0	4716	4706	5362
2021	CD	14.9	12.9	13.9	26.0	26.4	25.4	5443	4706	5061
	DB	12.4	12.9	14.6	19.6	26.4	27.3	4510	4706	5320
	DCBB	15.3	12.9	14.4	23.8	26.4	25.2	5568	4706	5266

Table 2 — Statistical error for Janakpur

Year	Model	MBE (MJ/m^2/day)	RMSE (MJ/m^2/day)	MPE (%)	r	CRM (MJ/m^2/day)	R^2
	BC	1.77	3.98	16.51	0.71	-0.05	0.57
2024	CD	2.14	4.89	37.01	0.72	-0.22	0.63
	DB	1.82	3.57	14.71	0.71	-0.04	0.66
	DCBB	2.01	3.54	20.27	0.77	-0.08	0.69
	BC	1.87	4.37	-23.57	0.75	-0.04	0.54
2023	CD	2.28	4.83	-24.05	0.76	-0.04	0.48
	DB	1.92	4.03	-21.55	0.73	-0.04	0.61
	DCBB	2.01	3.91	19.16	0.79	-0.03	0.62
	BC	-0.01	3.79	-5.30	0.77	0.09	0.54
2022	CD	-0.03	4.41	-3.41	0.78	0.13	0.46
	DB	-0.05	3.80	-6.56	0.75	0.09	0.57
	DCBB	0.03	3.54	-6.78	0.81	0.10	0.63
	BC	3.16	4.63	-21.19	0.62	-0.14	0.36
2021	CD	2.86	4.91	-15.98	0.61	-0.08	0.29
	DB	-9.85	4.78	24.57	0.43	-0.13	0.33
	DCBB	3.17	4.44	23.03	0.62	-0.12	0.37

0.41 (2024). By contrast, the lowest values were observed in winter, with 9.10 ± 0.35 (2021), 11.26 ± 0.45 (2022), 10.48 ± 0.37 (2023), and 10.22 ± 0.39 (2024), reflecting the effects of increased cloud cover and rainfall. The seasonal variation of GSR during 2021–2024, along with the associated errors, is presented in Table 3.

At the monthly scale, maximum GSR occurred in April 2024 (21.17 ± 0.44), June 2023 (21.64 ± 0.92), May 2022 (20.27 ± 0.66), and April 2021 (17.92 ± 0.66). Minimum values were recorded in January, with 7.30 ± 0.60 (2024), 7.96 ± 0.67 (2023), 8.52 ± 0.75 (2022), and 6.68 ± 0.53 (2021). Daily extremes were also significant: the highest solar radiation occurred on August 2, 2021 (26.45 MJ/m²/day), July 28, 2022 (28.34), June 2, 2023 (27.75), and June 23, 2024 (26.44), whereas the lowest were observed on January 16, 2021 (1.51), June 28, 2022 (2.27), May 2, 2023 (0.86), and September 28, 2024 (1.27). The monthly GSR for 2021–2024 with associated errors is presented in Table 4.

Temperature records indicated the hottest days as April 20, 2021 (38.5 °C), April 14, 2022 (39.5 °C), June 9, 2023 (42.5 °C), and April 30, 2024 (42.4 °C). The coldest were February 3, 2021 (5 °C), January 16, 2022 (6.5 °C), January 10, 2023 (6.5 °C), and January 29, 2024 (5 °C). Similarly, the wettest days were October 20, 2021 (116.3 mm), August 2, 2022 (100.3), August 8, 2023 (90.6), and July 2, 2024 (127.7). Peak wind speeds were recorded on July 31,

Table 3 — Seasonal GSR with error[16,22]

Seasons	GSR 2021	GSR 2022	GSR 2023	GSR 2024
winter	9.10 ± 0.35	11.26 ± 0.46	10.48 ± 0.37	10.22 ± 0.39
spring	15.80 ± 0.47	19.52 ± 0.30	19.22 ± 0.55	19.63 ± 0.41
summer	13.68 ± 0.53	18.44 ± 0.57	16.81 ± 0.69	17.92 ± 0.54
autumn	12.92 ± 0.38	15.93 ± 0.34	12.26 ± 0.54	13.35 ± 0.54

Table 4 — Monthly GSR with error[22]

Months	GSR 2021	GSR 2022	GSR 2023	GSR 2024
January	6.68 ± 0.54	8.52 ± 0.75	7.97 ± 0.67	7.30 ± 0.60
February	11.99 ± 0.55	15.22 ± 0.55	13.10 ± 0.51	12.91 ± 0.75
March	15.77 ± 0.49	18.77 ± 0.33	17.45 ± 0.80	17.65 ± 0.71
April	17.92 ± 0.67	19.52 ± 0.51	19.15 ± 0.80	21.17 ± 0.44
May	13.77 ± 1.04	20.28 ± 0.66	21.08 ± 1.11	20.12 ± 0.78
June	13.66 ± 0.94	17.31 ± 0.93	21.64 ± 0.92	18.29 ± 0.93
July	14.19 ± 0.81	19.70 ± 1.01	15.35 ± 0.96	17.61 ± 1.10
August	13.19 ± 0.99	18.27 ± 1.01	13.59 ± 1.20	17.87 ± 0.72
September	14.79 ± 0.78	16.18 ± 0.67	16.40 ± 1.00	15.19 ± 1.40
October	12.49 ± 0.64	17.55 ± 0.57	8.75 ± 0.65	13.49 ± 0.53
November	11.49 ± 0.31	13.99 ± 0.29	11.74 ± 0.50	11.38 ± 0.41
December	8.91 ± 0.30	10.44 ± 0.48	10.62 ± 0.29	10.44 ± 0.38

Table 5 — Seasonal average wind speed and rainfall[23]

Seasons	Average Mean Speed (m/s)				Rainfall (mm)			
	2021	2022	2023	2024	2021	2022	2023	2024
winter	1.48	1.86	1.94	1.49	11.30	85.01	0.00	0.71
spring	2.58	3.00	2.74	2.63	309.82	237.23	85.75	149.1
summer	2.99	3.34	3.27	3.05	1199.88	610.78	608.21	821.16
autumn	2.05	1.85	1.31	1.71	354.47	231.63	47.65	378.23

2021 (7.81 m/s), August 15, 2022 (8.02), June 27, 2023 (7.72), and August 2, 2024 (8.26). The seasonal average wind speed and rainfall are presented in Table 5.

Figures 2-9 illustrate the performance of the DCBB model and the meteorological dynamics influencing GSR in Janakpur during 2021-2024. The strong linear correlation between measured and estimated GSR (Fig. 2) confirms the model's robustness. Transmissivity variations and daily radiation patterns (Fig. 3) highlight short-term atmospheric effects, while ΔT trends (Fig. 4) show the role of thermal variability. Seasonal and monthly distributions (Figs. 6-7) reveal distinct cycles, with higher radiation in pre- and post-monsoon periods during the four years. Precipitation (Fig. 8) and wind speed (Fig. 9) further demonstrate seasonal climatic variability. Comparative analysis (Fig. 5) validates the DCBB model as a reliable tool for solar energy assessment in the Eastern Terai.

3.4 Correlation Analysis of Meteorological Variables and GSR

Correlation analysis was used to quantify the individual relationships between GSR and the major meteorological variables. Temperature and sunshine duration generally showed positive relationships with GSR, whereas rainfall and relative humidity showed negative relationships. The magnitude of these relationships varied among the variables, indicating their differing contributions to GSR variability at Janakpur. The individual relationships are presented graphically in Figs. 5-8.

The average GSR at Janakpur (4.11 ± 0.08 kWh/m²/day ≈ 14.80 ± 0.30 MJ/m²/day) is slightly lower than Jiri (15.05 MJ/m²/day)[22], likely due to Jiri's higher altitude and clearer atmosphere. It is also lower than Dhankutta (15.10 MJ/m²/day)[23, 24], Taplejung (15.17 MJ/m²/day)[25, 26], and Okhaldhunga (15.17 MJ/m²/day)[27], where reduced atmospheric thickness enhances solar radiation. Compared to Biratnagar (14.97 MJ/m²/day)[28], Janakpur shows very similar values, reflecting comparable Terai climatic conditions. However, it is higher than Kathmandu (13.55 MJ/m²/day)[29], where valley effects, fog, and air pollution reduce radiation. Janakpur is significantly lower than Jumla (19.58 MJ/m²/day)[30] due to the strong influence of high altitude and clear skies in the Himalayan regions.

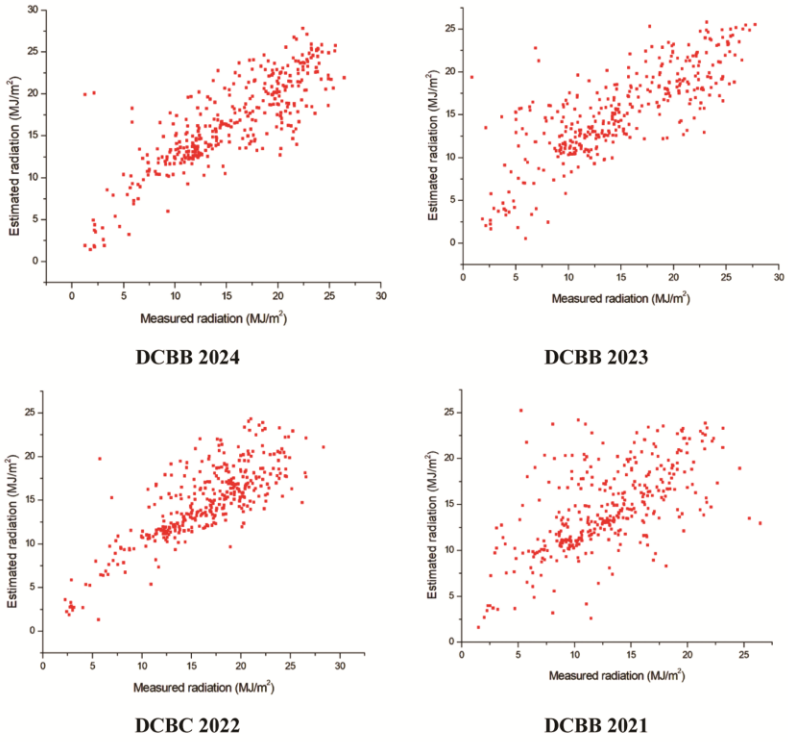


Fig. 2 — Linear relationship analysis of measured and estimated GSR data at Janakpur for 2021-2024 by Modular DCBB

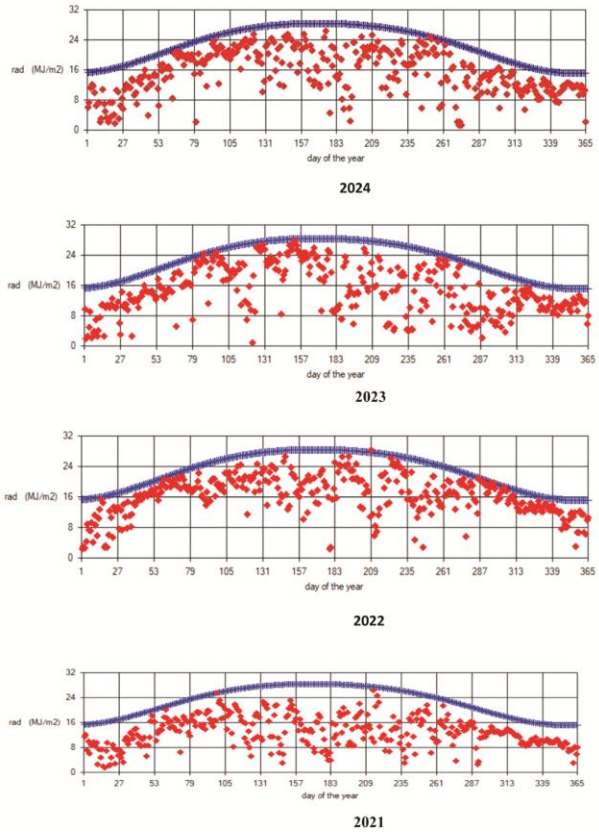


Fig. 3 — Daily fluctuations in GSR at Janakpur for 2021-2024

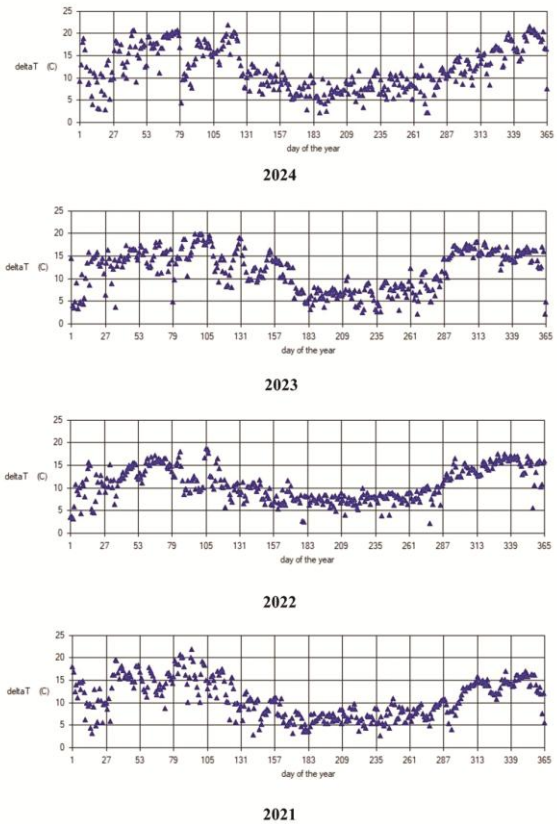


Fig. 4 — Daily fluctuations in delta T at Janakpur for 2021-2024

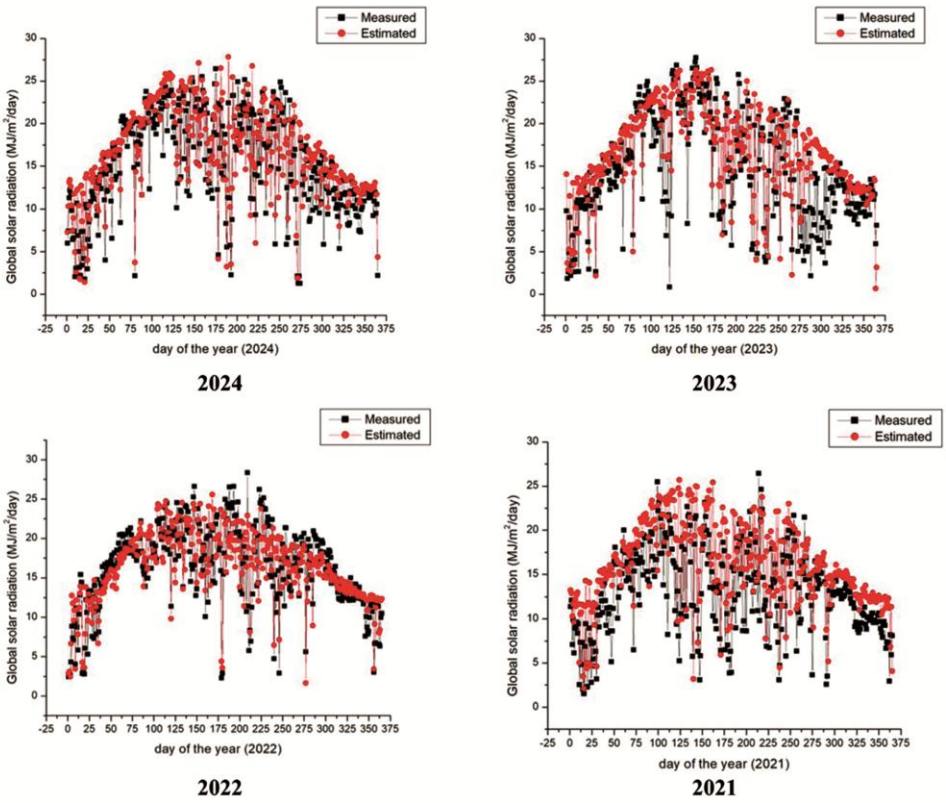


Fig. 5 — variation of measured and estimated GSR at Janakpur for 2021-2024

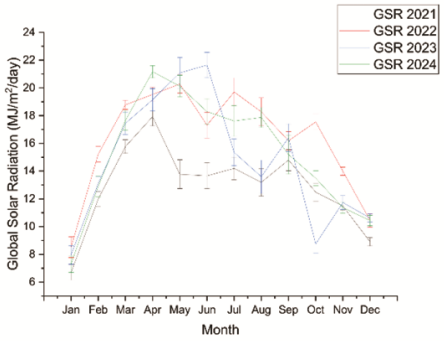


Fig. 6 — Seasonal Fluctuation of GSR at Janakpur

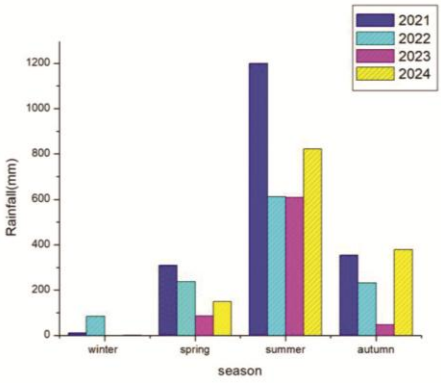


Fig. 8 — Seasonal Fluctuation of Precipitation at Janakpur

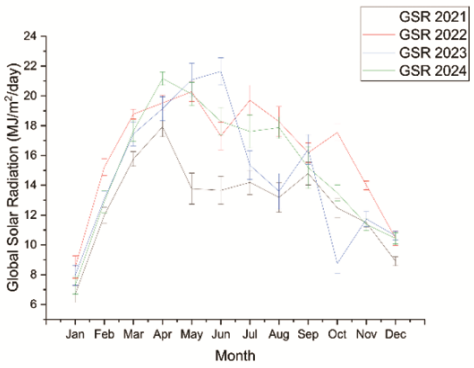


Fig. 7 — Monthly Fluctuation of GSR at Janakpur

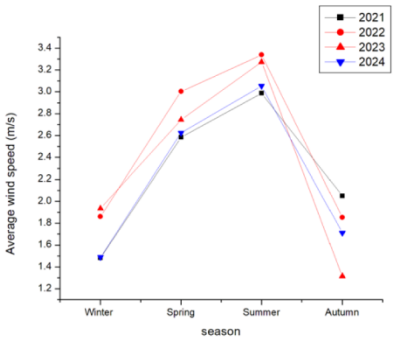


Fig. 9 — Seasonal Fluctuation of average wind speed at Janakpur

In global comparison, Janakpur is slightly higher than New York (14.07 MJ/m²/day) and Hong Kong (13.52 MJ/m²/day)[31], but much lower than Cairo (19.92 MJ/m²/day), Amman (20.51 MJ/m²/day), and Juba (19.66 MJ/m²/day)[32], where dry climates and minimal cloud cover result in higher solar radiation.

4 Discussion

4.1 Model Performance

The four RadEst models (BC, CD, DB, and DCBB) were evaluated by comparing estimated and observed GSR using MBE, RMSE, MPE, *r*, R^2, and CRM. Among the models, DCBB showed the best overall performance for Janakpur. It recorded the lowest RMSE in all four years (3.54-4.44 MJ m^{-2} day^{-1}) and the highest R^2 in three years, while also showing the highest or joint-highest *r* values throughout the study period. These results indicate better agreement and lower prediction errors than the other models. Therefore, based on the combined statistical indicators presented in Table 2, DCBB was identified as the best-performing model for estimating GSR at Janakpur.

4.2 Seasonal and Meteorological Influences

Seasonal variations in GSR at Janakpur are associated with rainfall, cloud cover, humidity, and atmospheric conditions. GSR is generally higher during spring and post-monsoon periods due to clearer skies and lower humidity, while winter values are reduced by low solar elevation, fog, and haze. During summer and monsoon periods, increased rainfall and cloud cover attenuate incoming solar radiation. The higher rainfall in 2024 (1349 mm) compared with 2022-2023 (approximately 610 mm) also coincided with lower GSR.

Among the meteorological parameters, rainfall appears to be the dominant influence on GSR in the lowland Terai region, mainly through its association with cloud cover and atmospheric moisture. Temperature and sunshine duration also influence GSR, while higher humidity generally reduces solar radiation. Thus, the seasonal and interannual variability of GSR is largely associated with rainfall-cloud conditions, particularly during the monsoon.

Future changes in rainfall, cloudiness, humidity, and extreme weather events associated with climate change may alter the availability and seasonal distribution of solar radiation in the Terai. Changes in monsoon timing and intensity could increase uncertainty in seasonal solar-energy yield, highlighting the need to consider climatic variability in long-term planning.

5 Conclusion

This study demonstrates that Janakpur in Nepal's Eastern Terai has moderate and relatively consistent solar radiation potential, indicating suitability for grid-connected and off-grid solar energy applications. Among the four empirical models evaluated using RadEst 3.0, the DCBB model generally provided the best overall performance for the study period, particularly in terms of correlation and error statistics. However, the moderate R^2 values indicate that the models have limited-to-moderate predictive capability and should therefore be used with appropriate consideration of local meteorological variability. The results suggest that the DCBB model can provide a useful empirical approach for preliminary GSR estimation in low-altitude Terai environments, but further calibration with longer and more representative ground-based observations is required for improved accuracy.

Local meteorology and topography, particularly temperature, rainfall, humidity, and post-monsoon clear skies, play a significant role in shaping solar radiation patterns, highlighting the importance of region-specific modelling for energy planning.

These findings have direct implications for solar energy development in Janakpur, supporting system design, resource assessment, and policy decisions aimed at expanding renewable energy access. Future work should focus on expanding ground-based measurements across the Terai, integrating machine learning approaches, and refining predictive models to further improve solar resource assessments and optimise solar energy deployment.

References

1 Shrestha J N, Bajracharya T, Shakya S & Giri B, *Renew energy Nepal-progress*, (2003) 12–14.
2 WECS, *Energy Sector Synopsis Report*, (2024) 22-28.
3 AEPC, *Annual Progress Report FY 2079/80*, (2024) 63-66.
4 Joshi U, Karki I B, Chapagain N P & Poudyal K N *BIBECHANA*, 18 (1) (2021) 159.
5 Dhakal S, Gautam Y & Bhattarai A, *Adv Meteorol*, (2020) 1–11.
6 Angström A, *Q J R Meteorol Soc*, 50 (210) (1924) 121.
7 Iqbal M, *An Introduction Solar Radiation*, Academic Press, New York,1983, p. 390.
8 Allen R G, *J Hydrol Eng*, 2 (2) (1997) 56.
9 Hassan G E, Youssef M E, Mohamed Z E, Ali M A & Hanafy A A, *Appl Energy*, 2016, p.179.
10 Li H, Cao F, Wang X & Ma W, *Sci World J*, (2014) 1.
11 Nage G D, *Int J Energy Environ Sci*, 3 (1) (2018) 19.

12 Olomiyesan B, Oyedum O, Ugwuoke P & Abolarin M, *Open Access J Photo Energy*, 1 (1) (2017) 1.
13 Oulimar I, Bouchouicha K, Bailek N & Bellaoui M, *Theor Appl Climatol*, 155 (4) (2024) 3493.
14 Pinto J S & Duarte SN, *Rev Bras Eng Agric Ambient*, 28 (6) (2024) 277.
15 Chhetri B R K & Gurung S, *Int J Syst Assur Eng Manag*, 8 (2) (2017) 1527.
16 Joshi U, Poudyal K N, Karki I B & Chapagain N P, *J Nepal Phys Soc*, 6 (1) (2020) 16.
17 Vanlalchhuanawmi C, Deb S, Islam M M & Ustun T S, *Int J Hydrogen Energy*, 50 (3) (2025) 198.
18 Tandon A, Awasthi A, Pattnayak K C, *et al*., *Discover Appl Sci*, 7 (2025) 107.
19 Donatelli M & Bellocchi G, *Institute Biometeorol CNR, Florence, Italy*, (2001) pp 213–214.
20 Donatelli M, Bellocchi G & Fontana F, *Eur J Agron* 18 (3) (2003) 363.
21 Donatelli M & Campbell G S, *European Soci Agronomy, Nitra, Slovakia*, 2 (1998) 133.
22 Rajbanshi B K, Singh R G, Rajbanshi A K S & K C B R, *Indian J Pure Appl Phys*, 64 (2026) 435.
23 Rajbanshi B K, Singh R G, K C B R & Poudel K N, *J Nepal Phys Soc*, 10 (1) (2024) 70.
24 Rajbanshi B K, Singh R G, K C B R, Joshi U & Poudyal K N, *J Nepal Phys Soc*, 11 (1) (2025) 1.
25 Rajbanshi B K, Singh R G, Khatiwada K, Thapa A, Kharel B & K C B R, *J Inf Syst Eng Manag*, 10 (16s) (2025) 716.
26 Rajbanshi B K, Singh R G, Rajbanshi A K S & K C B R, *J Insti Sci Tech, 31* (1) (2026) 107.
27 Rajbanshi B K, Singh R G, Kharel B, Thapa A & Khatiwada K, *Int'l J Env Sci, 11* (7s) (2025) 92.
28 Rajbanshi B K, Singh R G, Khatiwada K, Thapa A & K C B R, *Nanotechnol Percept*, 20 (16s) (2024) 1502.
29 Dawadi N, Shrestha M K, Khatri K, Poudyal K N, Karki I B & Tiwari B R, *BIBECHANA*, 23 (1) (2026) 31.
30 Kharel B, Thapa A, Khatiwada K, Rijal S, Rajbanshi B K & Poudyal K N, *J Inf Syst Eng Manag*, 10 (44s) (2025) 1013.
31 Al-Salameh A, *et al*., *Int J Energy Environ Sci*, 10 (4) (2025) 13.
32 Deng J M, Muot D Y & Mawien P P, *Energy Sustain Soc*, 15 (2025) 42.